

# High temperature spherical nano-indentation of graphite crystals

T.J. Marrow<sup>a,\*</sup>, I. Šulak<sup>b</sup>, B.-S. Li<sup>a</sup>, M. Vukšić<sup>a</sup>, M. Williamson<sup>a</sup>, D.E.J. Armstrong<sup>a</sup>

<sup>a</sup> Department of Materials, University of Oxford, UK

<sup>b</sup> Institute of Physics of Materials, Czech Academy of Sciences, Brno, Czech Republic

## ARTICLE INFO

### Article history:

Received 19 April 2021

Received in revised form

21 November 2021

Accepted 30 January 2022

Available online 3 February 2022

### Keywords:

Graphite

Nanoindentation

Kink band

High temperature

## ABSTRACT

Nano-indentation at temperatures up to 600 °C has been applied to the (0001) surface of highly oriented pyrolytic graphite using a spherical diamond tip (~10 μm diameter). Cross-sectional observations of the indentations by dark field scanning transmission electron microscopy show an increased tendency at high temperature for inelastic deformation by buckling of the graphite crystals with kink formation.

© 2022 The Authors. Published by Elsevier Ltd. This is an open access article under the CC BY license (<http://creativecommons.org/licenses/by/4.0/>).

## 1. Introduction

Synthetic polygranular graphite is a critical material for neutron moderation in advanced gas cooled nuclear fission reactors [1] and systems such as a Molten Salt Reactor [2], in which it will experience neutron irradiation and coolant interactions at temperatures of 600 °C and above. In the current AGR (Advanced Gas-cooled Reactors) the graphite temperatures approach 650 °C [3], and in high temperature gas cooled reactors, the graphite may be exposed to temperatures up to 900 °C, with inlet temperatures from 300 to ~500 °C [4]. It will also be exposed to static and dynamic loading from thermal and irradiation gradients and external forces that have potential to cause structural failures [5]. To assure the structural integrity and safe economic lifetime of advanced reactors, it is critical to understand how high temperature and irradiation will affect their materials.

Polygranular graphite is a complex material. In the unirradiated state its room temperature elastic properties are non-linear [6] and this is attributed to mechanisms including microcracking [7,8] that can cause the elastic modulus to decrease with increasing tensile strain [7]. Its thermal expansion and the temperature dependence of its elastic modulus are both influenced by fine scale microstructure features ('Mrozovski' accommodation pores [9]), which depend on the raw materials and processing of its manufacture; the

elastic modulus can increase with increasing temperature due to closure of these microscopic pores by thermal expansion [10]. Interactions with fast neutrons cause graphite crystal dimensional change, which also closes the fine pores, and other changes in physical properties [11]; in particular irradiation removes the non-linearity of polygranular graphite elastic deformation [12] and affects its fracture behaviour [13].

Despite a general understanding of the various synergistic mechanisms involved [12,14] it is not possible yet to predict how the properties of the graphite components will evolve in high temperature fission reactor environments. In particular, a better understanding of graphite deformation mechanisms is required. The tensile strength and fracture toughness of unirradiated polygranular graphite both increase at high temperature (up to 850 °C) [15,16], but there are no mechanical data reported for irradiated graphite at high temperature. A recent study of unirradiated polygranular graphite that measured total and elastic strains simultaneously by imaging and neutron diffraction [16] found a marked improvement in the ability to accommodate tensile strain at temperatures of 600 °C and above. It was proposed this may be due to an increased resistance to the propagation of crack-like defects within the microstructure. The mechanism for this is unclear, but the ability of the graphite crystals to accommodate inelastic deformation may be a factor.

Nano-indentation of single crystals [17] has shown graphite can deform at room temperature with kink band formation. This mechanism may depend on mobile basal dislocations [17,18], and a universal 'ripplocation' model has been proposed [19]. MAX phase

\* Corresponding author.

E-mail address: [james.marrow@materials.ox.ac.uk](mailto:james.marrow@materials.ox.ac.uk) (T.J. Marrow).

ceramics have layered structures, with similarity to graphite, and exhibit quite similar deformation mechanisms [20,21] that can cause a brittle-to-ductile transition at higher temperature [22]. However, there are no high temperature studies reported for graphite crystal deformation. This paper reports the first investigation of the deformation of graphite crystals at high temperature (up to 600 °C). Highly oriented pyrolytic graphite (HOPG) has a structure of basally-aligned crystallites [23] that is closely comparable to that observed in polygranular synthetic graphites [24,25], and has been used as a model material for the crystal behaviour (i.e. thermal and irradiation-induced dimensional change) of synthetic graphites [14,26]. It is used here to investigate the deformation of graphite crystals under well defined conditions. Cross-sectional characterization by high resolution transmission electron microscopy (TEM) has been performed on nano-indentations, with a spherical diamond tip, applied to highly oriented pyrolytic graphite (HOPG) at temperatures up to 600 °C.

## 2. Method

The specimen of SPI Grade-1<sup>1</sup> HOPG, measuring 10 × 10 × 1 mm, was from the batch studied by Wen [23]. It is a calibration-grade material with a lateral grain size of typically up to about 3 mm and a mosaic spread angle of about 0.4°. The larger surface that was oriented parallel to the graphite (0001) basal plane was cleaned by adhesive tape stripping [27] prior to nano-indentation, which was performed using a Micro Materials NanoTest<sup>TM</sup> Xtreme [28] located in a vacuum chamber (~10<sup>-6</sup> mbar). The indentations, using a spherical diamond tip with a nominal 10 µm diameter to avoid radial cracking, were conducted in load-controlled mode to peak loads from 5 to ~100 mN (20 s loading time at a constant rate, 5 s hold time). Temperature matching of the sample and indenter were conducted prior to each test to within 1 °C in order to minimise thermal drift. The same specimen was indented at increasing temperature up to 600 °C, separating the indents by at least 200 µm. The relationship between indentation depth ( $h_{tot}$ ) and effective tip radius ( $R$ ) was calibrated up to 900 nm depth on fused silica (Young's modulus, 72 GPa) via the load partial-unload method (up 128 mN, 5 s loading and unloading time, 2 s hold time).

The indentation elastic modulus,  $E_s$ , was obtained with the assumption of Hertzian elasticity and small contact depth using the contact load,  $P$ , and total indentation depth,  $h_{tot}$ , which is twice the depth over which the indenter tip and elastically deformed sample surface are assumed to be conformal [29],

$$\frac{P}{\pi a^2} = \frac{4}{3\pi} E^* \frac{a}{R} \quad (1)$$

$$h_{tot} = \frac{a^2}{R} \quad (2)$$

$$H_e = \frac{P}{\pi a^2} \quad (3)$$

$$\frac{1}{E^*} = \frac{1 - \nu_s^2}{E_s} + \frac{1 - \nu_i^2}{E_i} \quad (4)$$

where  $E^*$  is the reduced indentation modulus, with Poisson ratio ( $\nu$ ) and Young modulus ( $E$ ) having subscripts  $i$  and  $s$  that refer to the indenter and specimen respectively. The indentation stress,  $H_e$ , was obtained from the pressure of the contact load on the projected

elastic contact area of radius  $a$ . For Diamond,  $\nu_i$  and  $E_i$  were taken as 0.07 and 1170 GPa [29] and  $\nu_s$  was 0.24 [30] for HOPG, so the difference between reduced indentation modulus and specimen modulus is less than 4%.

Cross-section lamella for TEM analysis were prepared in a dual beam Tescan Lyra 3 FEG-SEM (field emission gun scanning electron microscope). The indents were protected by a platinum layer, applied using electron then ion deposition. Rough milling (gallium ions at 30 keV, 1–4 nA) produced a parallel-sided wall (1.5 × 10 µm) near the indent centre that was removed, platinum welded to an OmniProbe<sup>TM</sup> grid, fine milled (at ± 1.5°) to electron-transparency (Ga<sup>+</sup>, 30 keV, 0.1–1 nA) and then polished (Ga<sup>+</sup>, 5 keV, 250 pA). The lamellae were examined in a JEOL JEM-2100F transmission electron microscope operating at 200 kV in TEM (bright field, BF) and scanning (STEM) modes, using dark field (DF) imaging with a high-angle annular dark field (HAADF) detector. The camera length was 400 mm with the beam direction parallel to the basal plane.

## 3. Results

The nano-indentation load-displacement data (Fig. 1a) show similar deformation behaviour from room temperature to 300 °C. At 500 °C and above, there is a marked decrease in the load vs indentation displacement gradient, significant displacement jumps ('pop-in') at lower loads and hysteresis; after unloading (e.g., Fig. 1b), there tends to be a residual offset in the displacement. At 400 °C, both behaviours are observed. Some displacement jumps were very significant, reaching the displacement limit of the nanoindenter. The load-displacement traces for each indentation, with the target peak load and load at which the first significant displacement jump (if any) occurred, are presented in the Supplementary Information. The indentation stress,  $H_e$ , as a function of nominal indentation strain,  $\frac{4}{3\pi}(a/R)$ , is presented in Fig. 2 for loading only prior to any significant displacement jump. The same data for indentation stress are presented in the Supplementary Information as a function of indentation depth (up to 1000 nm). From room temperature to 400 °C, the effective moduli are close to 15 GPa; one room temperature indent shows high modulus, and one 400 °C indent has a low modulus. At 500 °C, the effective modulus decreases significantly with increasing nominal strain, most significantly when the contact stress is in the range of 1.5–2 GPa. At 600 °C, the effective modulus approaches 7.5 GPa, and then becomes almost zero for contact stresses in the range of 1.2–1.7 GPa. At high nominal strains, the effective moduli at all temperatures tend to increase towards 15 GPa. The 400 °C outlier shows behaviour that is similar to the indentations at 500° and 600 °C.

There is a large increase in the indentation imprint size at 600 °C (Fig. 3), with material laterally and vertically displaced around the indentation. At lower temperatures, the depth of the residual impression is small, with some disruption of the surface. In the example indentations at 50 mN peak load (Fig. 1b), for which the indentation depth up to 400 °C is approximately 1500 nm, the elastic contact radius,  $a$ , is calculated to be ~1500 nm; this is comparable to the dimensions of the imprints up to about 400 °C, with significantly larger imprints observed at higher temperature for the same maximum load (Fig. 3). At higher loads, there was very significant surface disruption from the large displacement jumps in which the indenter travelled to displacements exceeding 10,000 nm.

The specimen indentation modulus,  $E_s$ , which has been calculated during loading only and before any observable displacement jump, is presented in Fig. 4a for displacements up to the indenter calibration depth of 1000 nm; the nominal indentation strain at

<sup>1</sup> SPI Supplies (Structure Probe, Inc), West Chester, PA 19381-0656, USA.

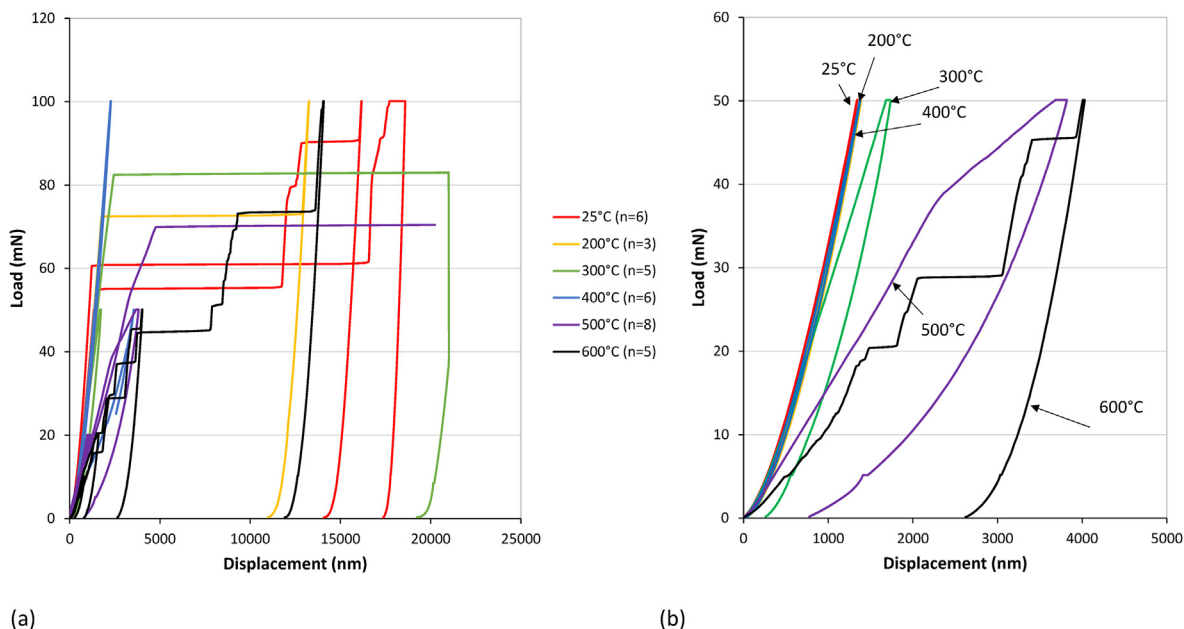


**Fig. 1.** Load-indentation displacement data for spherical nanoindentation of HOPG between 25 °C and 600 °C: a) data to different peak loads showing increased tendency for load-displacement jumps (‘pop-in’) at high temperature ( $n$  = number of indentations at the temperature); b) example data for single indentations obtained during loading to 50 mN peak load with unloading, for the indentations that are imaged in Fig. 3. (A colour version of this figure can be viewed online.)

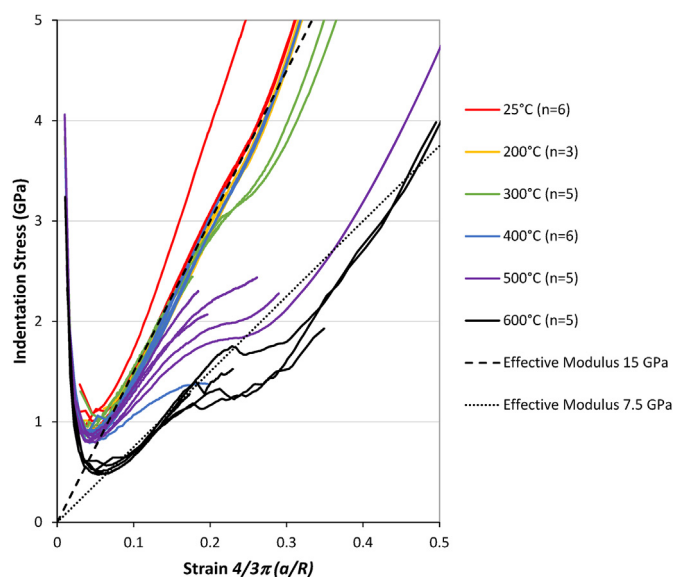


**Fig. 2.** The relationship between indentation stress and nominal indentation strain,  $4/3\pi(a_p/R)$ , as a function of temperature during loading. Reference lines for moduli of 15 and 7.5 GPa are shown. The nominal strain at 1000 nm displacement is  $\sim 0.26$ . (A colour version of this figure can be viewed online.)

this depth is approximately 0.26. Relatively stable values are obtained for indentation depths above  $\sim 100$  nm. The same data, averaged for each indentation over the displacement ranges of 200–300, 500–600 and 800–900 nm, are presented in Fig. 4b to show more clearly the effect of temperature. The indentation modulus data are presented individually for each temperature in the Supplementary Information.  $E_s$  is approximately constant ( $\sim 12$ – $15$  GPa) with indentation depth and temperature up to 400 °C with some outlier observations; one room temperature indent shows high indentation modulus approaching 20 GPa, and one 400 °C indent has a low modulus of  $\sim 8.5$  GPa. At 500 °C,  $E_s$

decreases significantly with increasing indentation depth towards  $\sim 7$ – $9$  GPa. At 600 °C,  $E_s$  is low ( $\sim 5$ – $8$  GPa) and insensitive to the indentation depth.

The TEM observations of the cross-sectional lamellae (Fig. 5a) show some inter-crystalline cracking approximately  $0.5 \mu\text{m}$  beneath the room temperature indentation that is parallel to the basal plane and the indented surface. There is a deformed zone with kinked crystals immediately adjacent to the indentation, but otherwise no deformation is observed elsewhere in the examined lamella. At 200 °C and above, there is a larger zone adjacent to the indentations with obvious kinks in the crystals (Fig. 5b), but no inter-crystalline cracks are observed except those associated with kink deformation. At 600 °C, the size of the zone of kink formation and inter-crystalline cracking adjacent to the indentation is significant (Fig. 5c). There are no other inter-crystalline cracks observed.

#### 4. Discussion

Relatively stable data for the specimen indentation elastic modulus are obtained for penetration depths above 100 nm, with very high modulus obtained at small penetration depths. This is consistent with previous room temperature nano-indentation studies of HOPG [31]. The room temperature indentation modulus of 12–15 GPa (Figs. 2 and 4a) is comparable to previous studies that reported values of 12–13 GPa [31] and 10.5 GPa [32]. An early study of pyrolytic graphite by spherical nanoindentation reported an effective indentation modulus of 7.5 GPa, with some non-recoverable deformation [33]. That study obtained the modulus from the relationship of the contact stress to strain, which was defined simply as the ratio of the elastic contact radius to the effective tip radius, and correcting here to the specimen indentation modulus (equations (1) and (4)) gives a value of 16.9 GPa. Variability between individual indents in HOPG has previously been attributed to local effects from the roughness of the cleaved surface [31]. This may explain the outlier measurement at 25 °C that has high modulus and high hardness.

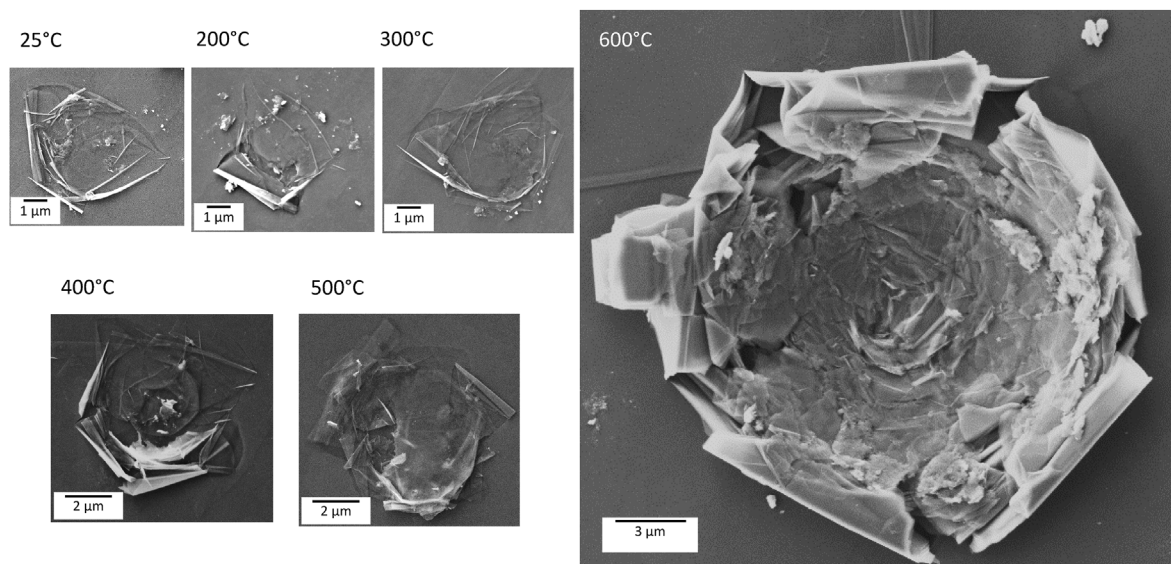


**Fig. 3.** Scanning electron microscope observations of indentations (all at 50 mN peak load) from room temperature to 600 °C, showing increased residual deformation at high temperature (600 °C). The load-indentation displacement data for these indents are shown in Fig. 1b. (Note, these images are presented at the same magnification).

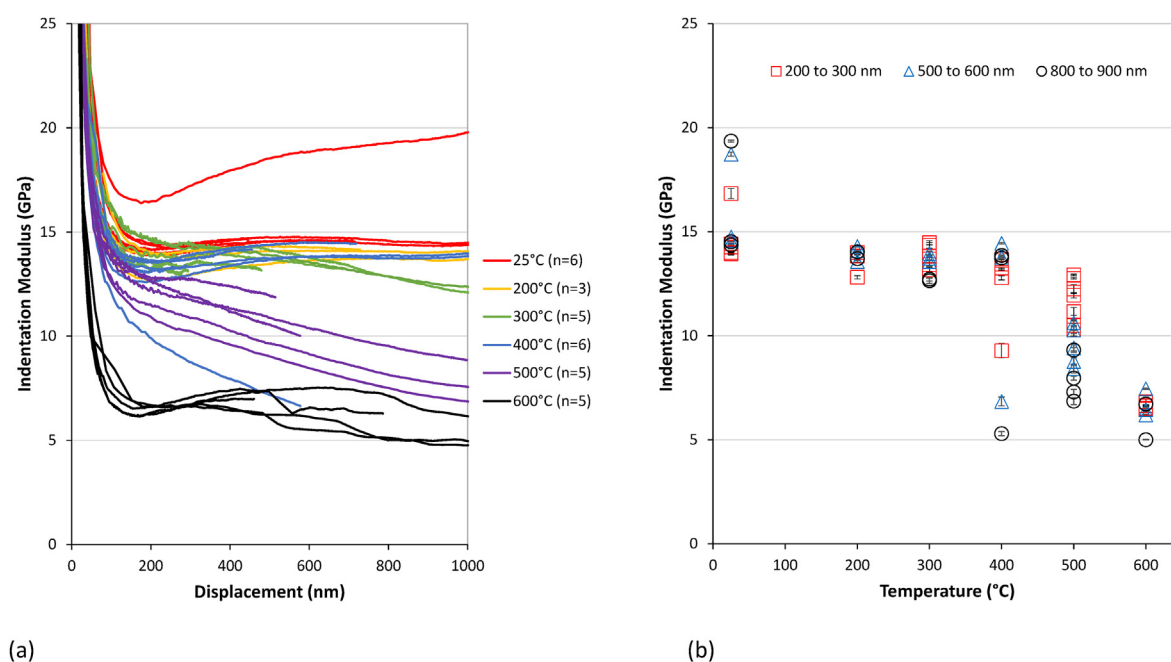


**Fig. 4.** Specimen indentation elastic modulus,  $E_s$ , measured by spherical indentation with the assumption of Hertzian contact at temperatures between 25 °C and 600 °C: a) indentation modulus as a function of indentation displacement ( $n$  = number of analysed indentations); b) effect of temperature on the average indentation modulus over selected ranges of indentation depth (displacement) for the data presented in (a). Error bars are one standard deviation for each indentation. (A colour version of this figure can be viewed online.)

The indentation modulus reduces towards ~7.5 GPa as the temperature is increased to 600 °C, and at both 500 °C and 600 °C, the modulus decreases with increasing strain, which is a characteristic of a secondary (i.e., inelastic or plastic) deformation mechanism. The modulus then increases significantly with increasing strain (Fig. 2) as the indentation depth exceeds 1000 nm, and approaches 15 GPa at high strains. It is speculated that this indentation behaviour at 500 °C and 600 °C might show the capacity for inelastic deformation has been exhausted and that elastic behaviour dominates with increasing displacement – this would be consistent with the plastic penetration of the indenter being

accommodated by lateral displacement of the material in layers surrounding the indenter at the unconstrained sample surface (e.g., Fig. 5c).

At room temperature, lateral buckling of the graphite crystals is observed to occur with kink formation, both on the surface (Fig. 3) and in the TEM cross-section of the nano-indentation (Fig. 5a). This inelastic deformation occurs to accommodate the penetration of the indenter [31,34] (Fig. 1a). Buckling with kinking has been observed previously in graphite [17,35]. Ion irradiation has also been observed to induce kink bands in HOPG, possibly to accommodate irradiation-induced dimensional change [36]. Here, at



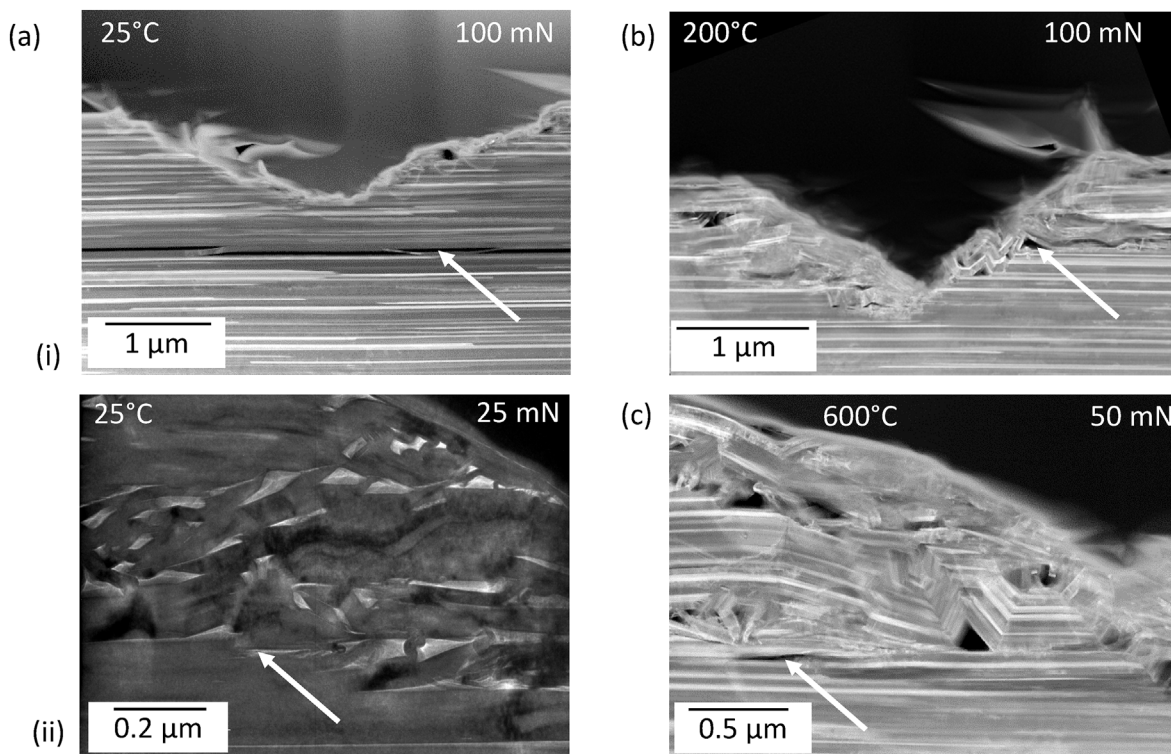


**Fig. 5.** Transmission electron microscopy of indentation cross-section lamellae that show increasing zone of kink formation with increasing temperature: a) room temperature [(i) HAADF (ii) BF (bright field)]; b) 200 °C [HAADF]; c) 600 °C [HAADF]. (white arrows indicates inter-crystalline cracks).

room temperature, it occurs within a zone that is immediately adjacent to the indentation. It becomes more widespread at higher temperatures (Fig. 5b and c), simultaneously with increased indentation imprints (Fig. 3) and residual deformation (Fig. 1b). The physical significance of the indentation moduli, which are obtained by analysis of the load-penetration data with the assumptions of elastic behaviour and Hertzian contact, may be affected by the surface buckling. Nonetheless, the present analysis provides an approximate means to investigate the effect of temperature on the deformation of the graphite crystals. The nominal stress/strain relationships (Fig. 2) and indentation modulus (Fig. 4) demonstrate there is a change in indentation behaviour above around 400 °C, with a reduction in the effective hardness of the surface.

The large displacement jumps (pop-ins) during loading (Fig. 1) are instabilities associated with unstable buckling by kinking of the graphite crystals that are aligned parallel to the indented surface (Fig. 1a). Similar discontinuities have been observed in room temperature indentation of graphite [17,32] and these should not be confused with the smaller pop-ins commonly observed in nano-indentation of metallic crystals that are due to nucleation of dislocations [37]. At higher temperatures, the plastic deformation becomes more widespread (Fig. 5b), and the low indentation moduli at 500 °C and 600 °C are a consequence of propagation of significant plastic deformation by stable buckling of the surface crystals adjacent to the indentation (i.e., continuous yielding without visible displacement jump). There is a clear transition in the indentation behaviour as the temperature increases above 400 °C. The outlier indentation at 400 °C with low modulus and hardness approaches the behaviour at 500 °C and may arise from a local reduction in the resistance to the initiation of buckling.

Lateral cracking beneath indentations can occur due to tensile residual stresses that develop on removal of the indenter [38] because of the inelastic deformation surrounding the indentation. This residual stress is sufficient to cause inter-crystalline cracking of

graphite beneath the indentation at room temperature (Fig. 5a). The absence of inter-crystalline cracks at higher temperature indicates lower magnitude residual stresses, despite the more extensive inelastic deformation. This is consistent with the inelastic deformation occurring at lower stress with increasing temperature and the lateral accommodation of the indenter by increasingly widespread buckling.

No significant change in the bulk elastic properties of graphite is expected over the studied temperature range up to 600 °C [39–41]. The present data do not allow this to be confirmed reliably through analysis of the unloading behaviour particularly at high temperature, as the significant surface disruption during loading may affect the contact area. Continuous stiffness measurement (CSM) with oscillating load, together with future studies that investigate the effects of the geometry of the indenter (e.g., radius of curvature) might allow this to be verified.

This study shows that inelastic buckling by kink formation in graphite crystals occurs with increasing ease at elevated temperatures during spherical nanoindentation. The kinks in the graphite crystal are similar to those observed in MAX phase ceramics [20,21], and may occur by the same mechanism [19]. Easy shear, by processes such as basal dislocation glide, is required for buckling in layered structures [21]. The instability that leads to buckling depends on the interaction between the shear and elastic bending stiffness of the layers. The resistance to basal dislocation glide in graphite is extremely low [42–44] and this manifests as its low shear modulus,  $C_{44}$  [42,45]. There are no data for the effects of high temperature (i.e., up to 600 °C) on the elastic constants of graphite single crystals. However, over the range from room temperature to 4 K, the elastic constant,  $C_{33}$  (for compression perpendicular to the basal plane) has been observed in HOPG to decrease with increasing temperature [46]. In that study the value of  $C_{33}$  and its temperature dependence were sample independent, as expected, but the value of  $C_{44}$  was sample dependent, as was its response to

temperature. It has also been deduced from high temperature studies of polycrystalline graphite that the shear modulus,  $C_{44}$ , varies with the degree of crystallite order and is affected by graphite processing [47]. In general, the value of  $C_{44}$  in graphite is understood to be strongly affected by pinning of basal dislocations by crystal defects [42], particularly irradiation-induced point defects [48]. We propose that the temperature dependence of graphite crystal deformation by buckling that is observed in this study is due to an effect of temperature on the value of  $C_{44}$ , relative to  $C_{33}$  and  $C_{11}$  (i.e., the stiffnesses of the graphite crystals perpendicular and parallel to the basal plane that are less affected by temperature).

The change in indentation behaviour above 400 °C in HOPG occurs with easier buckling of the graphite crystals, and the transition occurs around this temperature for this geometry of spherical indentation onto the basal plane. A decrease in  $C_{44}$  with increasing temperature, such as by thermally activated basal dislocation glide, would facilitate the development of kinking and buckling of graphite crystals that are compressed laterally during indentation. Polygranular graphite has a domain structure similar to the HOPG structure of aligned graphite crystals [24], so a similar transition may occur around, but not necessarily at, this temperature as graphite processing affects the shear modulus [47]. Neutron irradiation also strongly affects the properties of graphite crystals [12], particularly the shear modulus [48]. Irradiation may therefore be expected to affect the conditions for kinking and buckling to occur, with possible consequences on the general ability of polygranular graphites to deform inelastically. To understand how neutron irradiation may affect the high temperature structural integrity of graphite components, studies of irradiated graphite are imperative. As a first step, high temperature nano-indentation of ion-radiated HOPG might be used to investigate the temperature dependence of the underlying mechanisms of kink band formation and buckling. Such studies might also elucidate the effects of temperature and strain rate on thermally activated shear, and should also investigate the annealing of irradiation-induced defects that act as barriers to shear deformation.

## 5. Conclusions

Spherical nano-indentation onto the basal plane of highly oriented pyrolytic graphite (HOPG) causes the graphite crystals to deform inelastically by buckling with kink formation. The propensity and ease of buckling increases with increasing temperature. It is hypothesised this due to the greater effect of temperature on the shear modulus,  $C_{44}$ , which is sensitive to the pinning of basal dislocations, than the axial moduli (i.e.,  $C_{33}$  and  $C_{11}$ ). The introduction and annealing of defects such as those induced by irradiation is expected to influence the temperature and strain rate dependence of the buckling mechanism, and should be further investigated.

## CRedit authorship contribution statement

**T.J. Marrow:** Conceptualization, Supervision, Writing – original draft, Writing – review & editing. **I. Sulak:** Investigation. **B.-S. Li:** Investigation. **M. Vukšić:** Investigation. **M. Williamson:** Investigation, Writing – review & editing. **D.E.J. Armstrong:** Investigation, Writing – review & editing.

## Declaration of competing interest

The authors declare that they have no known competing financial interests or personal relationships that could have appeared to influence the work reported in this paper.

## Acknowledgements

The authors acknowledge use of characterization facilities within the David Cockayne Centre for Electron Microscopy, Department of Materials, University of Oxford. TJM acknowledges the support of the EPSRC Advanced Materials for Nuclear Fission programme under UNIGRAF: Understanding and Improving Graphite for Nuclear Fission (EP/M018679/1). IS acknowledges the support of the Czech Academy of Sciences. MV acknowledges receipt of Frankopan Scholarships (STA920 and STA889) from the Frankopan Fund (The Staples Trust). MW acknowledges an Industrial CASE EPSRC studentship (18000117) with support from NNL and EDF Energy Generation.

## Appendix A. Supplementary data

Supplementary data to this article can be found online at <https://doi.org/10.1016/j.carbon.2022.01.067>.

## References

- [1] J.P. Bonal, A. Kohyama, J. Van Der Laan, L.L. Snead, Graphite, ceramics, and ceramic composites for high-temperature nuclear power systems, *MRS Bull.* 34 (2009) 28–34.
- [2] R.W. Moir, Recommendations for a restart of molten salt reactor development, *Energy Convers. Manag.* 49 (2008) 1849–1858, <https://doi.org/10.1016/j.enconman.2007.07.047>.
- [3] I.R. Cameron, The Gas-Cooled Graphite-Moderated Reactor. Nuclear Fission Reactors, Springer US, Boston, MA, 1982, pp. 227–247, [https://doi.org/10.1007/978-1-4613-3527-6\\_8](https://doi.org/10.1007/978-1-4613-3527-6_8).
- [4] B.J. Marsden, Nuclear Graphite for High Temperature Reactors, International Atomic Energy Agency (IAEA), 2001.
- [5] J. Knott, 4 - nuclear power plants: types, components and material requirements, in: A. Shirzadi, S. Jackson (Eds.), *Structural Alloys for Power Plants*, Woodhead Publishing, 2014, pp. 69–101, <https://doi.org/10.1533/9780857097552.1.69>.
- [6] S. Yoda, M. Eto, T. Oku, Change in dynamic young's modulus of nuclear-grade isotropic graphite during tensile and compressive stressing, *J. Nucl. Mater.* 119 (1983) 278–283, [https://doi.org/10.1016/0022-3115\(83\)90204-0](https://doi.org/10.1016/0022-3115(83)90204-0).
- [7] T.J. Marrow, D. Liu, S.M. Barhli, L. Saucedo-Mora, Y. Vertyagina, D.M. Collins, et al., In situ measurement of the strains within a mechanically loaded polygranular graphite, *Carbon* 96 (2016) 285–302, <https://doi.org/10.1016/j.carbon.2015.09.058>.
- [8] D. Liu, K. Mingard, O.T. Lord, P. Flewitt, On the damage and fracture of nuclear graphite at multiple length-scales, *J. Nucl. Mater.* 493 (2017) 246–254, <https://doi.org/10.1016/j.jnucmat.2017.06.021>.
- [9] S. Mrozowski, Mechanical strength, thermal expansion and structure of cokes and carbons, in: *Proc. 1st and 2nd Conferences on Carbon*, Waverly Press, Buffalo, NY, 1956, p. 31.
- [10] I.B. Mason, R.H. Knibbs, Variation with temperature of young's modulus of polycrystalline graphite, *Nature* 188 (1960) 33–35, <https://doi.org/10.1038/188033a0>.
- [11] B.T. Kelly, Graphite—the most fascinating nuclear material, *Carbon* 20 (1982) 3–11, [https://doi.org/10.1016/0008-6223\(82\)90066-5](https://doi.org/10.1016/0008-6223(82)90066-5).
- [12] J.E. Brocklehurst, B.T. Kelly, Analysis of the dimensional changes and structural changes in polycrystalline graphite under fast neutron irradiation, *Carbon* 31 (1993) 155–178, [https://doi.org/10.1016/0008-6223\(93\)90169-B](https://doi.org/10.1016/0008-6223(93)90169-B).
- [13] X. Jin, J. Wade-Zhu, Y. Chen, P.M. Mummery, X. Fan, T.J. Marrow, Assessment of the fracture toughness of neutron-irradiated nuclear graphite by 3D analysis of the crack displacement field, *Carbon* 171 (2021) 882–893, <https://doi.org/10.1016/j.carbon.2020.09.072>.
- [14] B.J. Marsden, M. Haverty, W. Bodel, G.N. Hall, A.N. Jones, P.M. Mummery, et al., Dimensional change, irradiation creep and thermal/mechanical property changes in nuclear graphite, *Int. Mater. Rev.* 61 (2016) 155–182, <https://doi.org/10.1080/09506608.2015.1136460>.
- [15] D. Liu, B. Gludovatz, H.S. Barnard, M. Kuball, R.O. Ritchie, Damage tolerance of nuclear graphite at elevated temperatures, *Nat. Commun.* 8 (2017), <https://doi.org/10.1038/ncomms15942>.
- [16] D. Liu, T. Zillhardt, P. Earp, S. Kabra, T. Connolly, Marrow J. In situ measurement of elastic and total strains during ambient and high temperature deformation of a polygranular graphite, *Carbon* 163 (2020) 308–323, <https://doi.org/10.1016/j.carbon.2020.03.020>.
- [17] M.W. Barsoum, A. Murugiah, S.R. Kalidindi, T. Zhen, Y. Gogotsi, Kink bands, nonlinear elasticity and nanoindentations in graphite, *Carbon* 42 (2004) 1435–1445, <https://doi.org/10.1016/j.carbon.2003.12.090>.
- [18] S. Basu, A. Zhou, M.W. Barsoum, On spherical nanoindentations, kinking nonlinear elasticity of mica single crystals and their geological implications, *J. Struct. Geol.* 31 (2009) 791–801, <https://doi.org/10.1016/j.jsg.2009.05.008>.

- [19] M.W. Barsoum, X. Zhao, S. Shanazarov, A. Romanchuk, S. Koumlis, S.J. Pagano, et al., Ripplations: a universal deformation mechanism in layered solids, *Phys. Rev. Mater.* 3 (2019), 013602, <https://doi.org/10.1103/PhysRevMaterials.3.013602>.
- [20] B.J. Kooi, R.J. Poppen, N.J.M. Carvalho, J.T.M. De Hosson, M.W. Barsoum, Ti<sub>3</sub>SiC<sub>2</sub>: a damage tolerant ceramic studied with nano-indentations and transmission electron microscopy, *Acta Mater.* 51 (2003) 2859–2872, [https://doi.org/10.1016/S1359-6454\(03\)00091-0](https://doi.org/10.1016/S1359-6454(03)00091-0).
- [21] G. Plummer, H. Rathod, A. Srivastava, M. Radovic, T. Ouisse, M. Yildizhan, et al., On the origin of kinking in layered crystalline solids, *Mater. Today* 43 (2021) 45–52, <https://doi.org/10.1016/j.mattod.2020.11.014>.
- [22] M.W. Barsoum, M. Radovic, Elastic and mechanical properties of the MAX phases, *Annu. Rev. Mater. Res.* 41 (2011) 195–227, <https://doi.org/10.1146/annurev-matsci-062910-100448>.
- [23] K. Wen, J. Marrow, B. Marsden, Microcracks in nuclear graphite and highly oriented pyrolytic graphite (Hopg), *J. Nucl. Mater.* 381 (2008) 199–203, <https://doi.org/10.1016/j.jnucmat.2008.07.012>.
- [24] B. März, K. Jolley, T.J. Marrow, Z. Zhou, M. Heggie, R. Smith, et al., Mesoscopic structure features in synthetic graphite, *Mater. Des.* 142 (2018) 268–278, <https://doi.org/10.1016/j.matdes.2018.01.038>.
- [25] K.Y. Wen, T.J. Marrow, B.J. Marsden, The microstructure of nuclear graphite binders, *Carbon* 46 (2008) 62–71, <https://doi.org/10.1016/j.carbon.2007.10.025>.
- [26] B. Marsden, A. Mummery, P. Mummery, Modelling the coefficient of thermal expansion in graphite crystals: implications of lattice strain due to irradiation and pressure, *Proc. Math. Phys. Eng. Sci.* 474 (2018) 20180075, <https://doi.org/10.1098/rspa.2018.0075>.
- [27] A.K. Geim, Nobel lecture: random walk to graphene, *Rev. Mod. Phys.* 83 (2011) 851–862, <https://doi.org/10.1103/RevModPhys.83.851>.
- [28] J.M. Wheeler, D.E.J. Armstrong, W. Heinz, R. Schwaiger, High temperature nanoindentation: the state of the art and future challenges, *Curr. Opin. Solid State Mater. Sci.* 19 (2015) 354–366, <https://doi.org/10.1016/j.cossms.2015.02.002>.
- [29] A. Murugaiah, M.W. Barsoum, S.R. Kalidindi, T. Zhen, Spherical nano-indentations and kink bands in Ti<sub>3</sub>SiC<sub>2</sub>, *J. Mater. Res.* 19 (2004) 1139–1148, <https://doi.org/10.1557/JMR.2004.0148>.
- [30] X. Meng, H. Zhang, J. Song, X. Fan, L. Sun, H. Xie, Broad modulus range nanomechanical mapping by magnetic-drive soft probes, *Nat. Commun.* 8 (2017) 1944, <https://doi.org/10.1038/s41467-017-02032-y>.
- [31] T.S. Gross, N. Timoshchuk, I. Tsukrov, R. Piat, B. Reznik, On the ability of nanoindentation to measure anisotropic elastic constants of pyrolytic carbon, *Zamm-Zeitschrift Fur Angewandte Mathematik Und Mechanik* 93 (2013) 301–312.
- [32] A. Richter, R. Ries, R. Smith, M. Henkel, B. Wolf, Nanoindentation of diamond, graphite and fullerene films, *Diam. Relat. Mater.* 9 (2000) 170–184, [https://doi.org/10.1016/S0925-9635\(00\)00188-6](https://doi.org/10.1016/S0925-9635(00)00188-6).
- [33] J.S. Fielda, M.V. Swain, The indentation characterisation of the mechanical properties of various carbon materials: glassy carbon, coke and pyrolytic graphite, *Carbon* 34 (1996) 1357–1366, [https://doi.org/10.1016/S0008-6223\(96\)00071-1](https://doi.org/10.1016/S0008-6223(96)00071-1).
- [34] P. Diss, J. Lamon, L. Carpentier, J.L. Loubet, P. Kapsa, Sharp indentation behavior of carbon/carbon composites and varieties of carbon, *Carbon* 40 (2002) 2567–2579, [https://doi.org/10.1016/S0008-6223\(02\)00169-0](https://doi.org/10.1016/S0008-6223(02)00169-0).
- [35] Z. Liu, Q. Zheng, J.Z. Liu, Stripe/kink microstructures formed in mechanical peeling of highly orientated pyrolytic graphite, *Appl. Phys. Lett.* 96 (2010) 201909, <https://doi.org/10.1063/1.3422484>.
- [36] D. Liu, D. Cherns, S. Johns, Y. Zhou, J. Liu, W.-Y. Chen, et al., A macro-scale ruck and tuck mechanism for deformation in ion-irradiated polycrystalline graphite, *Carbon* 173 (2021) 215–231, <https://doi.org/10.1016/j.carbon.2020.10.086>.
- [37] D. Lorenz, A. Zeckzer, U. Hilpert, P. Grau, H. Johansen, H.S. Leipner, Pop-in effect as homogeneous nucleation of dislocations during nanoindentation, *Phys. Rev. B* 67 (2003) 172101, <https://doi.org/10.1103/PhysRevB.67.172101>.
- [38] Y. Vertyagina, M. Mostafavi, C. Reinhard, R. Atwood, T.J. Marrow, In situ quantitative three-dimensional characterisation of sub-indentation cracking in polycrystalline alumina, *J. Eur. Ceram. Soc.* 34 (2014) 3127–3232, <https://doi.org/10.1016/j.jeurceramsoc.2014.04.002>.
- [39] S. Sato, Y. Imamura, K. Kawamata, J.-I. Kon, M. Ohtani, Studies on high temperature strength of graphite, *J. Soc. Mater. Sci. Japan* 20 (1971) 409–417, <https://doi.org/10.2472/jsms.20.409>.
- [40] T. Maruyama, M. Eto, T. Oku, Elastic modulus and bend strength of a nuclear graphite at high temperature, *Carbon* 25 (1987) 723–726, [https://doi.org/10.1016/0008-6223\(87\)90141-2](https://doi.org/10.1016/0008-6223(87)90141-2).
- [41] M. Li, J. He, Effect of high temperature on ultrasonic velocity in graphite, *Diam. Relat. Mater.* 116 (2021) 108368, <https://doi.org/10.1016/j.diamond.2021.108368>.
- [42] R.H. Telling, M.I. Heggie, Stacking fault and dislocation glide on the basal plane of graphite, *Phil. Mag. Lett.* 83 (2003) 411–421, <https://doi.org/10.1080/0950083031000137839>.
- [43] D.E. Soule, C.W. Nezbeda, Direct basal-plane shear in single-crystal graphite, *J. Appl. Phys.* 39 (1968) 5122–5139, <https://doi.org/10.1063/1.1655933>.
- [44] O.L. Blakslee, D.G. Proctor, E.J. Seldin, G.B. Spsnce, T. Weng, Elastic constants of compression-annealed pyrolytic graphite, *J. Appl. Phys.* 41 (1970) 3373–3382.
- [45] B.T. Kelly, *Physics of Graphite*, Applied Science, United Kingdom, 1981.
- [46] D.M. Hwang, The temperature dependence of the elastic constants for highly oriented pyrolytic graphite determined by ultrasonic techniques, *Solid State Commun.* 46 (1983) 177–181, [https://doi.org/10.1016/0038-1098\(83\)90605-1](https://doi.org/10.1016/0038-1098(83)90605-1).
- [47] I.B. Mason, R.H. Knibbs, The Young's modulus of carbon and graphite artefacts, *Carbon* 5 (1967) 493–506, [https://doi.org/10.1016/0008-6223\(67\)90026-7](https://doi.org/10.1016/0008-6223(67)90026-7).
- [48] E.J. Seldin, C.W. Nezbeda, Elastic constants and electron-microscope observations of neutron-irradiated compression-annealed pyrolytic and single-crystal graphite, *J. Appl. Phys.* 41 (1970) 3389–3400, <https://doi.org/10.1063/1.1659430>.